ACS Macro Letters

Letter

pubs.acs.org/macroletters

Nanorod Assemblies in Polymer Films and Their Dispersion-Dependent Optical Properties

Michael J. A. Hore,[†] Amalie L. Frischknecht,[‡] and Russell J. Composto*,[†]

[†]Department of Materials Science and Engineering and the Laboratory for Research on the Structure of Matter, University of Pennsylvania, Philadelphia, Pennsylvania 19104, United States

[‡]Center for Integrated Nanotechnologies, Sandia National Laboratories, P.O. Box 5800, MS 1411, Albuquerque, New Mexico 87185, United States

ABSTRACT: Optical absorption due to surface plasmon resonances in ensembles of gold nanorods (Au NRs) depends strongly on the nanorod separation and orientation. Here, we study the dispersion of polystyrene-functionalized Au NRs in polystyrene (PS) thin films using UV−visible (UV−vis) spectroscopy and transmission electron microscopy (TEM) and find that Au NRs are dispersed for brush chain lengths that exceed the PS matrix chain length and are aggregated otherwise. Monte Carlo simulations using parameters from classical density functional theory (DFT) calculations indicate that this behavior is due to substantial depletion−attraction forces for brush chain lengths that are much smaller than the PS matrix chain length. Both UV−vis measurements and discrete dipole approximation (DDA) calculations confirm that optical absorption is a facile method to determine nanorod morphology in nanocomposite films (i.e., aggregation or dispersion). Futhermore, a dispersion map is constructed showing the conditions required for nanorod dispersion and, correspondingly, the optical absorption properties of Au NR:PS nanocomposites. Using this information, optically active materials with tunable morphologies can be fabricated and routinely characterized using optical spectroscopic methods.

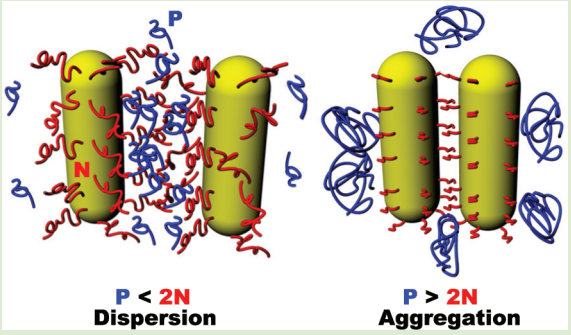

Combining the functionality of nanoparticles with the processability of polymers holds great promise for designing new magnetic, optical, and medical devices. For example, metallic nanoparticles can greatly enhance Raman scattering by surface plasmons resulting in an increase in sensitivity of up to 8 orders of magnitude. This enhanced sensitivity underpins the single molecule sensitivity of surface-enhanced Raman spectroscopy (SERS). Primarily, this enhancement depends strongly on the shape, proximity, and geometrical arrangement of the nanoparticles.[1,2] Compared to spheres, nanorods have the added advantage of exhibiting longitudinal (LSPR) and transverse (TSPR) surface plasmon resonances that strongly depend on the local orientation of neighboring nanorods. For example, by examining pairs of Au NRs on an indium tin oxide (ITO) substrate, Funston et al.[3] demonstrated that the LSPR wavelength would blue-shift or red-shift depending on whether the NRs are oriented side-by-side or end-to-end, respectively. These shifts were attributed to plasmon coupling between NR pairs located closer than three times their NR diameter. Although selected pairs of Au NRs on a surface have been investigated, the full potential of devices that utilize optically active particles has not been realized because a facile method to control their spacing and orientation is lacking.

Control over the dispersion and spacing of NRs would be a significant advance in the field of nanoparticle-based devices. One strategy to precisely control the location of particles is to fabricate them in a top-down fashion using electron beam lithography. However, this method is relatively slow and costly compared to exploiting the natural tendency of nanoparticles to self-assemble. To prevent aggregation and control their spacing, nanoparticles can be grafted with a polymer brush. The brush also allows one to tune the thermodynamic interactions between nanoparticles and a polymer host to direct the assembly of the nanoparticles via enthalpic and entropic interactions. For the former case (i.e., entropically dominated system), the nanoparticles may either uniformly disperse or aggregate, depending on the brush grafting density and relative length of the brush and matrix polymers. However, for the latter case (i.e., enthalpically dominated system), the nanoparticles uniformly disperse throughout the film, provided that the interaction between the brush and polymer matrix is favorable.[4] Because the LSPR wavelength and plasmon coupling strength depends strongly on NR separation and orientation, the dispersion of nanorods directly determines the optical activity of polymer nanocomposite films.

The dispersion or aggregation of nanoparticles is mainly determined by whether the brush on the nanoparticle is wet by the matrix polymer (i.e., matrix polymer penetrates into the

Received: August 19, 2011
Accepted: November 9, 2011
Published: November 23, 2011

   dx.doi.org/10.1021/mz200031g | *ACS Macro Lett.* 2012, 1, 115−121

brush layer). The earliest experimental work on autophobic dewetting goes back to Liu et al.[5] who found that a planar brush evolves from the wet to dry state as P increases above $P \approx 5N$, where P is the degree of polymerization of the matrix polymer and N is the degree of polymerization of the brush. A dry brush is observed if the conformational entropy loss of matrix chains within the brush leads to matrix chain expulsion or, correspondingly, depletion−attraction forces between brush-coated surfaces. Later, Bansal et al.[6] observed that the transition from dispersion to aggregation for polystyrene (PS) functionalized silica nanoparticles in a PS matrix occurred at a relatively lower value of P, when $P \approx 0.7N$. In this case, the window for wet brush (i.e., dispersed) conditions is greatly reduced relative to $P \approx 5N$. Early self-consistent field theory (SCFT) calculations showed that the boundary between wet and dry brush states in planar systems was observed near $P \approx N$.[7] When the effects of brush grafting density are considered, the boundary between wet and dry conditions is predicted as $\sigma(N)^{1/2} > (N/P)^2$.[8] More recent SCFT calculations found depletion−attraction forces at all values of P and N, but the attraction is only significant for sufficiently large values of P and grafting density σ. These calculations predict that the boundary scales roughly as $\sigma(N)^{1/2} \approx (N/P)^{0.7}$ for $P < 3N$.[9] Recently, Frischknecht[10] used a polymeric density functional theory (DFT) to calculate the forces between nanorods with adsorbed polymer chains in a chemically identical matrix and found that nanorods would experience an increasingly attractive force between each other as P/N increased. Using SCFT, Trombly and Ganesan[11] calculated the boundary between wet and dry brush regimes on spherical nanoparticles as a function of grafting density, P, and N. They observed a correlation between the strength of the interparticle attraction and the amount of interpenetration of the brush and matrix polymer chains and a weak dependence on the grafting density of the brush. Most importantly, the boundary between wet and dry brush regimes was shifted from that found in a planar system. When curvature becomes an important consideration, as is the case in nanorod composites, and the brush length N is constant, the transition between wet and dry brush regimes shifts to higher values of P relative to the planar case, increasing the window for wet brush conditions. This shift is due to the ability of the free chain-end to splay outward as the distance away from the curved nanorod surface increases. Under these conditions, the matrix polymer loses less conformational entropy and more readily penetrates into the brush layer. This enhancement in dispersion was observed by Kim and Green[12] where PS-functionalized Au nanospheres in PS were found to aggregate when $P > 3N$, which is higher than expected for a planar brush. The transition from wet to dry brush has not yet been investigated in nanorods dispersed in a polymer matrix.

Self-consistent field theories describing the interfacial properties between polymer brushes and matrix chains have been successful in capturing experimental studies of the wet to dry brush transition on planar and spherical surfaces. However, experimental studies themselves have reported different results about the relationship between brush and matrix length and this transition,[5,6,12] indicating that systematic experimental studies and their comparison to SCFT results are needed. The variability reported in the literature may be attributed to differences in nanoparticle type, brush grafting density, or the competition between bulk dispersion and surface segregation. Nanorods represent an interesting geometry for investigating the wet to dry brush transition because their shape is neither spherically symmetric nor planar. In the present study, a significant result is that the assembly, spacing, and orientation of PS-functionalized Au NRs in PS thin films can be controlled by varying the brush and matrix lengths (i.e., transitioning from a wet nanorod brush to a dry nanorod brush). Moreover, using transmission electron microscopy and optical absorption measurements, a quantitative analysis method is proposed to evaluate whether nanoparticles are well-dispersed (more than 90% individual NRs), partially dispersed, or aggregated (fewer than 50% individual NRs). In this way, we quantitatively investigate the effects of N and P on the dispersion of PS-functionalized Au NRs in a PS matrix and simultaneously compare our results to previous experimental work on planar and spherical nanoparticle systems. By analyzing the LSPR wavelength obtained from UV−visible spectroscopy measurements, we show for the first time that optical properties provide a simple and accurate route for evaluating the dispersion of Au NRs in a polymer matrix. Classical density functional theory (DFT) is used to determine interaction energies representative of partially ($\varepsilon = 5k_BT$) and aggregated ($\varepsilon = 10k_BT$) systems. Using these interaction energies, Monte Carlo simulations show that the side-by-side nanorod alignment observed by transmission electron microscopy (TEM) can be attributed to depletion−attraction forces. These results combined with discrete dipole approximation calculations indicate that side-by-side alignment is responsible for the blue-shift of the LSPR wavelength. Finally, a dispersion map plotting brush length versus matrix length identifies the combinations of N and P that produce well-dispersed and aggregated NRs as well as the chain lengths that define the transition between wet and dry brush states, $P = 2N$.

Figure 1 shows a gallery of TEM micrographs for all PS-Au(N):PS(P) films at fixed values of thickness, $d \approx 25$ nm, and NR volume fraction $\phi_{rod} \approx 0.05$. The left axis represents the degrees of polymerization of the PS brush (N = 48, 110, and 191), and the bottom axis refers to the degrees of polymerization of the PS matrix (P = 26 to 1459). From the gallery of images, two categories of dispersion are observed. First, for long brushes (namely, N = 110 and N = 191) in shorter matrix polymers of P = 26 and P = 173, the nanoparticles are mainly isolated from each other and appear well-dispersed. These dispersions are similar to those previously observed in films of poly(ethylene glycol)-functionalized (PEG) Au NRs in poly(methyl methacrylate) (PMMA).[4] However, whereas the rod−rod spacing is uniform in PEG-Au:PMMA, the distance between the Au NRs appears more random in PS-Au:PS. As the matrix chain length increases (i.e., $P \geq 384$), the nanorods are not well-dispersed and form aggregates containing side-by-side neighboring nanorods. This behavior is most striking at high matrix degree of polymerization (i.e., last column, P = 1459), though smaller NR aggregates are observed for P = 384 and P = 586. As N increases in the aggregated systems, the inter-rod spacing of the nanorods in the aggregates increases. This spacing between neighboring nanorods relative to the average nanorod radius is approximately r_{rod}, $2r_{rod}$, and $3r_{rod}$ for N = 48, 110, and 191, respectively. This increase in spacing is attributed to an increase in brush thickness as N increases. As expected for dry brushes,[8] the spacing scales as $\langle r \rangle \sim N$. Next, we examine whether these changes in NR spacing influence the optical properties.

For each brush length N, the optical absorption is measured using UV−vis spectroscopy and shown in Figure 2a−c. Each set of spectra shows the absorption in PS matrices of length P = 26

dx.doi.org/10.1021/mz200031g | ACS Macro Lett. 2012, 1, 115−121

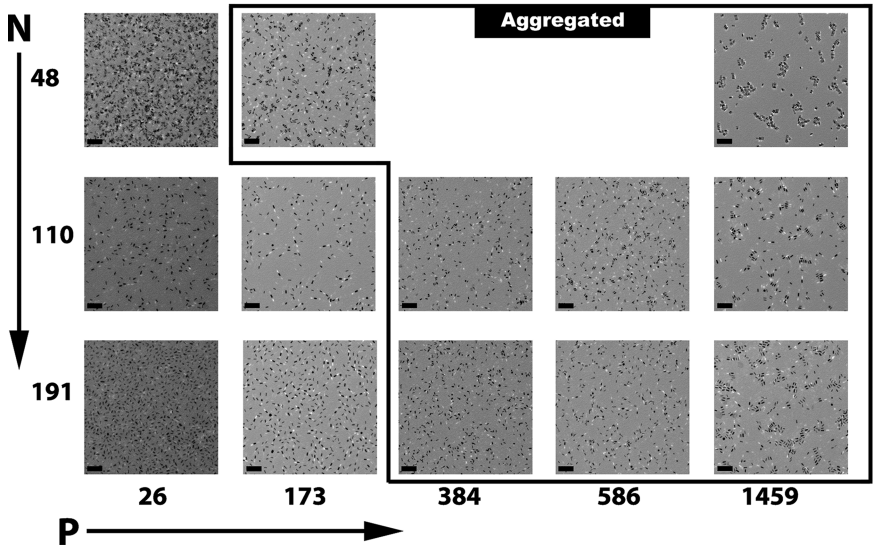

Figure 1. TEM images of PS-Au(N):PS(P) thin films as a function of PS brush length (N) and PS matrix length (P). For $P < N$, nanorods are dispersed randomly in the PS matrix. However, as P increases, the Au NRs partially aggregate and eventually aggregate at $P = 1459$. The Au NR volume fraction is ≈0.05. The scale bars are 200 nm.

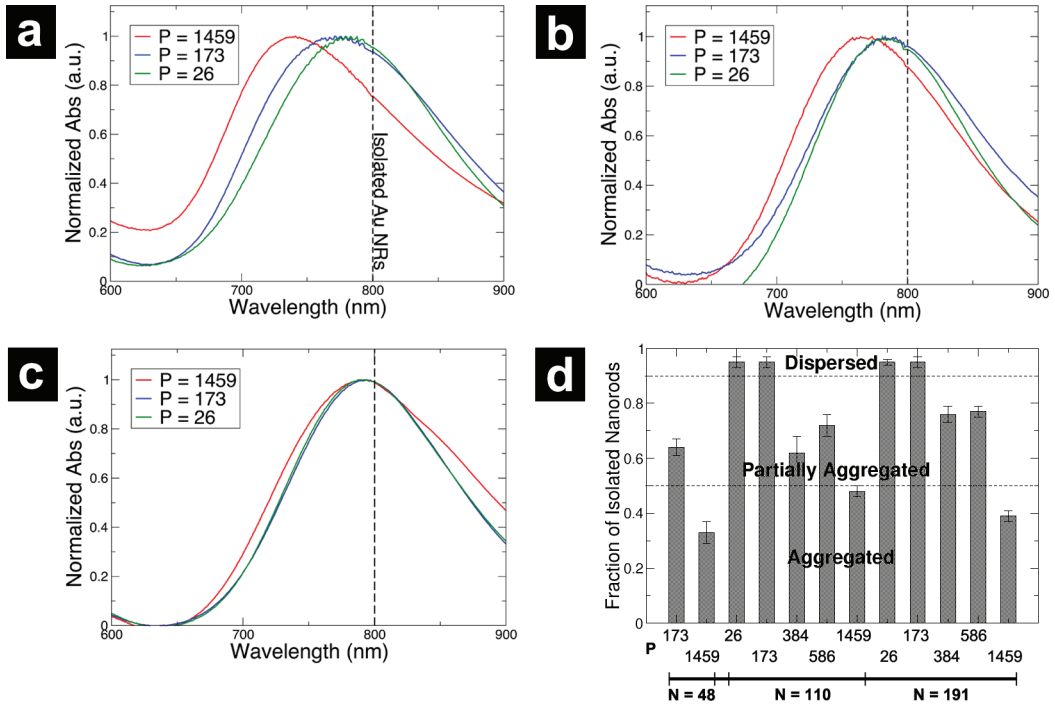

Figure 2. Optical and dispersion characterization of PS-Au(N):PS(P) films. The UV−vis spectra are shown for N = (a) 48, (b) 110, and (c) 191. The dashed line is the LSPR wavelength for isolated Au NRs in PS. As P increases from 26 to 1459, the LSPR peak becomes increasingly blue-shifted for $N = 48$ and $N = 110$. However, for $N = 191$, the nanorod separation is too large for plasmon coupling, and the LSPR does not shift. Nevertheless, significant peak broadening is observed for $P = 1459$, indicating that there is weak coupling between LSPRs, relative to a and b. As a means to quantify dispersion, part d shows that the fraction of isolated rods falls into three categories. Composites having >90% isolated rods are denoted as "dispersed", whereas films with less than 50% isolated rods are aggregated. Partially aggregated systems fall between 50% and 90%.

(green), 173 (blue), and 1459 (red), along with a reference line at $\lambda = 800$ nm, which represents the LSPR for isolated nanorods. For $N = 48$, Figure 2a shows that the LSPR wavelength blue-shifts as the molecular weight of the matrix increases, consistent with closer spacing and side-by-side alignment. The magnitude of the blue-shift depends on the relative values of P and N. For $N = 48$, the blue-shift is $\Delta\lambda \approx 30$ nm for both $P = 26$ and $P = 173$, whereas for $P = 1459$, the shift is even stronger and $\Delta\lambda \approx 60$ nm. For $N = 110$ and $P = 1459$, the LSPR position is blue-shifted by $\Delta\lambda \approx 35$ nm. For $N = 191$ the LSPR peak position remains fixed at $\lambda \approx 790$ nm (i.e., same as isolated Au NRs), though peak broadening is observed for the $P = 1459$ case. The optical properties reported in Figure 2a−c are consistent with the TEM micrographs in Figure 1, which show that Au NRs form aggregates consisting of side-by-side nanorods that grow in size as P increases. The relative

dx.doi.org/10.1021/mz200031g | ACS Macro Lett. 2012, 1, 115−121

orientation of the nanorods with respect to each other is responsible for the blue-shift of the LSPR. Note that the blue-shift is less pronounced at high N (e.g., compare Figure 2a and c) because the spacing between adjacent Au NRs increases as brush length increases.

To categorize the PS-Au(N):PS(P) films as aggregated or dispersed, the fraction of isolated nanorods in the TEM images is calculated. Figure 2d shows that the fraction of isolated nanorods for each PS-Au(N):PS(P) film falls into three distinct categories of dispersion. First, dispersed films are defined as having more than 90% of the nanorods as individual, isolated particles. These PS-Au(N):PS(P) films have a uniform dispersion of nanorods for the conditions $P \lesssim N$. Second, for $P \sim N$, the fraction of isolated nanorods decreases to between 50% and 90% because the nanorods begin to form aggregates. By examining the TEM images, the morphology of these "partially aggregated" systems corresponds to small aggregates of a few Au NRs coexisting with isolated nanorods. Finally, if $P \gg N$ (i.e., $P = 1459$), the Au NRs are defined as "aggregated" because more than 50% of the Au NRs are found in aggregates. Furthermore, compared to the partially aggregated morphology, the aggregate size is larger in the aggregated systems.

The dispersion of the nanorods obtained from our MC simulations can be compared to the experimentally observed morphologies shown in Figure 1. This comparison can be used to determine whether the estimated interaction energies reproduce the dispersed, partially aggregated, and aggregated morphologies defined in Figure 2d. Figure 3 shows the

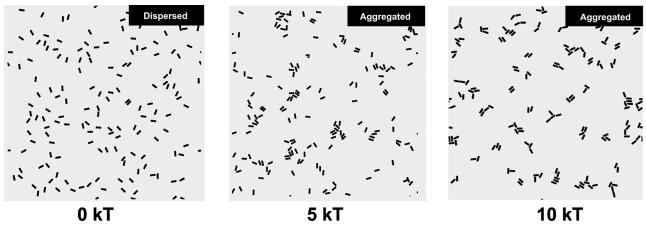

Figure 3. Monte Carlo configurations of nanorods as a function of increasing depletion–attraction energy (ε). As the inter-rod attraction increases, the morphology changes from dispersed to partially aggregated and finally to strongly aggregated. These interaction strengths represent PS-Au(N):PS(P) systems where $P < N$ ($0k_BT$), $P > N$ ($5k_BT$), and $P \gg N$ ($10k_BT$). Approximately 2×10^6 MC steps were used in each simulation. To match experimental results (Figure 1), $\phi_{rod} = 0.05$.

arrangement of nanorods ($\phi_{rod} = 0.05$) determined by the MC simulations for interaction energies of $\varepsilon = 0$, 5, and $10k_BT$, which correspond to the PS-Au(N):PS(P) systems having $P < N$, $P > N$, and $P \gg N$, respectively. Three distinct morphologies are observed that are consistent with the categories of dispersion identified by TEM analysis (Figure 2d). For $\varepsilon = 0$ (i.e., no interaction between nanorods), a very well-dispersed morphology is observed, with isolated nanorods distributed across the simulation space. As the interaction energy increases to $\varepsilon = 5k_BT$ (i.e., moderately attractive), a partially aggregated morphology is observed with small, loosely packed aggregates forming and coexisting with a small fraction of isolated nanorods. Correspondingly, the regions of pure polymer become larger because of the partial aggregation. When ε is small, the weak depletion–attraction interaction must compete with the translational entropy of the rods, which favors mixing. Thus, the driving force for aggregation is greatly reduced, resulting in a partially aggregated morphology. Finally, for strongly attractive nanorod interactions ($\varepsilon = 10k_BT$), a majority of the nanorods are located in aggregates, and few isolated nanorods are observed. For this case of $P \gg N$ the depletion–attraction force between NRs is large, leading to a mostly aggregated state. The simulated morphologies show mostly side-by-side aggregates of nanorods, rather than end-to-end aggregates, which is consistent with the TEM images of Figure 1.

Figure 4 shows the extinction efficiencies (Q_{ext}) for arrangements of nanorods that are representative of the morphologies observed in the MC simulations (Figure 3) and TEM (Figure 1). Recall that nanorods in the simulations are either dispersed or found in small loosely packed aggregates (partially aggregated) or larger closely packed aggregates (aggregated). To capture these morphologies, we calculate Q_{ext} for nanorod dimers, representing the small aggregates formed when $P \sim N$, and for nanorod tetramers, representing the large aggregates formed when $P \gg N$. For $N = 48$ (Figure 4a), nanorods in the aggregate are separated by a distance of approximately r_{rod}. The calculated spectra of Figure 4a are in good qualitative agreement with the experimental spectra shown in Figure 2a. For nanorods that are aligned side-by-side, a pronounced blue-shift in the LSPR wavelength is observed for dimers and tetramers from $\lambda_{LSPR} \approx 830$ nm for isolated nanorods to $\lambda_{LSPR} \approx 770$ nm and $\lambda_{LSPR} \approx 730$ nm, respectively. However, for $N = 110$ and 191, the NRs in aggregates are spaced farther apart because the increase in brush length increases the spacings between nanorods to $2r_{rod}$ and $3r_{rod}$, respectively. Correspondingly, the blue-shift in the LSPR position in Figure 4b (spacing = $2r_{rod}$) is less than that of Figure 4a (spacing = r_{rod}). Namely, the LSPR is shifted to approximately $\lambda_{LSPR} \approx 790$ nm for dimers and $\lambda_{LSPR} \approx 760$ nm for tetramers. A significant blue-shift in the LSPR is not observed for $N = 191$ (Figure 4c) because the adjacent nanorods are sufficiently far apart to preclude surface plasmon coupling.[3] These results are in qualitative agreement with the measured optical spectra in Figure 2a–c.

The agreement between the optical properties (UV–vis and DDA) and morphology studies (MC and TEM) demonstrates that the optical properties of polymer nanocomposites can be used to determine the dispersion of nanorods. Namely, the blue-shifts observed in the UV–vis spectra of Figure 2 reflect the quality of the Au NR dispersion. For instance, when nanorods are aggregated, their LSPR wavelength is shorter than that expected for isolated nanorods in polystyrene. As the quality of the Au NR dispersion decreases (i.e., the nanorods begin to aggregate in small and then larger aggregates), the LSPR wavelength undergoes a blue-shift because of the surface plasmon coupling between nanorods aligned side-by-side. For $P \gtrsim N$, the inter-rod interaction energy is weak, and nanorods will cluster into small aggregates as observed in the MC simulations and TEM images shown in Figures 3 and 1, respectively. For $P \gg N$, the nanorods are found almost exclusively in aggregates, resulting in a strong blue-shift in the LSPR. If the brush is very long (i.e., high N), the nanorod separation within the aggregates will be large, and therefore, the surface plasmons between neighboring nanorods will not strongly couple. In this case, only very small blue-shifts are observed in the LSPR position, even for highly aggregated nanorods. Note that because the DDA calculations assume monodisperse nanorods in a dimer or tetramer configuration, the peak broadening observed in experimental UV–vis spectra (Figure 2) is not reproduced.

dx.doi.org/10.1021/mz200031g | ACS Macro Lett. 2012, 1, 115–121

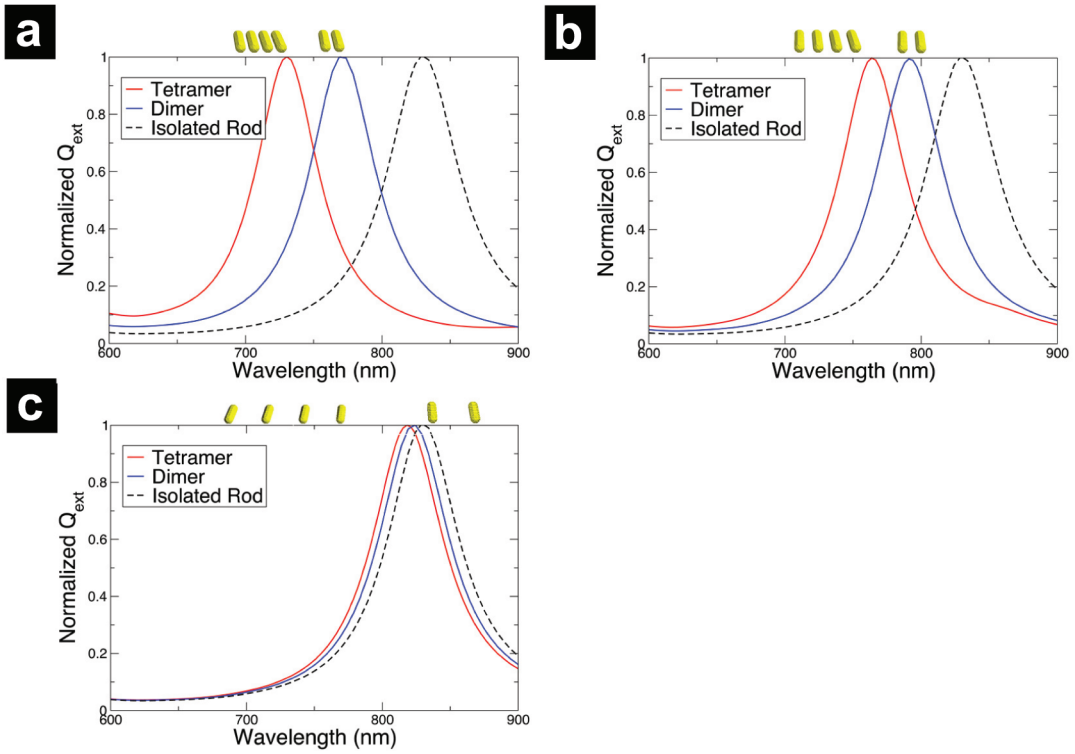

Figure 4. Discrete dipole approximation calculations of extinction efficiencies for side-by-side Au NR dimers (blue) and tetramers (red) in polystyrene for NR spacings of (a) r_{rod}, (b) $2r_{rod}$, and (c) $3r_{rod}$. For comparison, the extinction efficiency of isolated nanorods in PS (black dashed line) is also shown with a peak at 830 nm. The increase in spacing captures the increase in brush length, N. The peak in Q_{ext} corresponds to the surface plasmon resonance wavelength and, because of LSPR coupling, is increasingly blue-shifted for dimers and tetramers in a and b as compared to isolated NRs. For large NR spacings (e.g., part c), the coupling from individual NRs is weak, and therefore no significant shift is observed.

Nonetheless, the DDA simulations qualitatively reproduce the changes in optical properties observed in Figure 2, implying that the blue-shifts in the measured optical spectra result from an increase in side-by-side alignment of NRs.

The dispersion map in Figure 5 summarizes the NR morphology in the PS-Au(N):PS(P) systems (solid symbols) determined from TEM and UV−vis experiments. For completeness, we have also included dispersion data from poly(ethylene glycol) (PEG)-functionalized Au NRs in poly(ethylene oxide) (PEO) matrices (open symbols), which represents an attractive brush−matrix system.[4] Regardless of the chemical species of the nanocomposite, we observe two distinct regions corresponding to aggregation and dispersion, depending on P and N. The dashed line between the aggregated and the dispersed regions of the dispersion map is given by $P = 2N$. This result is in good agreement with experimental results from Kim and Green[12] for PS-functionalized Au nanospheres in PS and also SCFT calculations[11] which show that the boundary between aggregation and dispersion should occur at higher values of P than expected for planar systems. In particular, we observe the transition between dispersion and aggregation to fall between the conditions for planar surfaces ($P \approx N$) and spherical surfaces ($P \approx 3N$). In Figure 5, the half-shaded square represents PS-Au(48):PS(26), for which the TEM results were ambiguous with regards to the morphology of the NRs. Atomic force microscopy (AFM) analysis (not shown) indicates that the nanorods are mostly dispersed in the film, whereas the TEM images suggest both aggregation and dispersion of the NRs. To demonstrate the utility of using spectroscopic measurements alongside TEM or AFM imaging, we note that the blue-shift in the UV−vis spectrum in Figure 2a suggests that the nanorods in PS-Au(48):PS(26) are partially aggregated—a conclusion that could not be reached by using TEM or AFM alone. Hence, UV−vis spectroscopy can be used as a rapid screening tool to determine whether nanoparticles are dispersed or aggregated in polymer nanocomposite films.

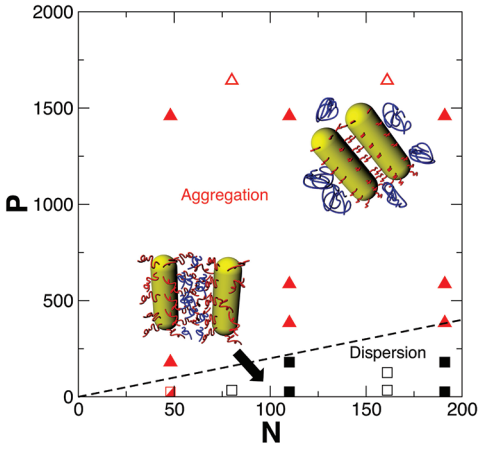

Figure 5. Dispersion map of PS-Au(N):PS(P) films showing how N and P determine NR morphology. Squares correspond to composites with isolated NRs that are dispersed in PS, and triangles correspond to NRs that form aggregates in PS. In addition to PS-Au(N):PS(P) (solid symbols), the morphology for the PEG-Au(N):PEO(P) system is also given (open symbols). The dashed line corresponds to $P = 2N$ and represents the transition between aggregation and dispersion. The morphology of PS-Au(48):PS(26) is ambiguous and represented by the half-shaded symbol.

dx.doi.org/10.1021/mz200031g | ACS Macro Lett. 2012, 1, 115−121

The present research demonstrates the strong correlation between nanoparticle dispersion and optical absorption. This connection was made by investigating nanorods in polymer films using images (TEM) and simulations (MC) to capture morphology and UV−vis and DDA to measure and interpret optical properties, respectively. Because nanoparticle shape has a strong effect on the wavelengths that excite surface plasmons, future studies should explore polymer nanocomposites containing nanowires, stars, and other shapes of nanoparticles. In addition, the NRs in the present study are globally isotropic in their orientation. To utilize their polarizing properties, the Au NRs can be aligned by applying an external force such as an electric field.[13] In addition to being a facile method to determine nanoparticle dispersion, the sensitivity (i.e., shifts) of UV−vis to nanorod spacing can be utilized in devices. For example, nanorod composite films can be used as SERS substrates, where control over the LSPR wavelength allows for very sensitive detection of single molecules.

METHODS

Au NR synthesis: In this study, Au NRs (volume fraction $\phi_{rod} \approx 0.05$) are incorporated into PS thin films (film thickness $d \approx 25$ nm). The Au NRs were synthesized using a seed-mediated growth method that has been described elsewhere.[4,14,15] The nanorods are approximately 12 × 42 nm. Reagents were obtained from Sigma Aldrich and used as received. Au NRs were then functionalized with thiol-terminated polystyrene (thiol-PS) (Polymer Source, Inc.). The molecular weights of the thiol-PS and their polydispersity indices were 5 kg/mol (1.10), 11.5 kg/mol (1.08), and 20 kg/mol (1.07). The functionalization was performed by first centrifuging approximately 45 mL of the as-synthesized Au NR solution for 60 min at 8000 rpm (Eppendorf Centrifuge 5804). The supernatant was discarded, and the precipitated Au NRs were redispersed in 250 μL of ultrapure H_2O (Millipore). This solution was then pipetted into 8 mL of a 2 mM thiol-PS/tetrahydrofuran (THF) solution and stirred for 24 h. The resulting solution was centrifuged for 30 min at 8000 rpm and the precipitate redispersed in 10 mL of toluene. Thiol-PS grafting densities were measured using thermogravimetric analysis, yielding values of σ = 0.28 and 0.15 chains/nm^2 for PS molecular weights of 11.5 kg/mol and 20 kg/mol, respectively. The 5 kg/mol grafting density was measured previously and found to be σ = 0.53 chains/nm^2.[16] A final centrifugation was performed before redispersing the Au NR precipitate in 1 mL of a 1 wt % polystyrene/toluene solution. The polystyrene had molecular weights of 2.7 kg/mol (PDI < 1.09, Pressure Chemical), 18 kg/mol (PDI < 1.07, Sigma Aldrich), 40 kg/mol (PDI = 1.05, Polymer Source, Inc.), 61 kg/mol (PDI = 1.05, Polymer Source, Inc.), and 152 kg/mol (PDI < 1.05, Pressure Chemical).

Sample preparation: For each brush (N) and matrix (P) length, PS-Au(N):PS(P) thin films were prepared by spin coating a Au NR/polystyrene solution on silicon for 60 s at 3000 rpm and drying overnight in a fume hood. These films had thicknesses of approximately 25 nm, as measured by ellipsometry (Rudolph AutoEL III) and X-ray reflectivity (Rigaku SmartLab). TEM specimens were prepared by scoring the film, floating off small portions in ultrapure H_2O, and picking up the pieces on holey carbon-coated TEM grids (mesh size 300, Structure Probe, Inc.). Because the 2.7 kg/mol thin film had a molecular weight below the entanglement molecular weight of polystyrene (≈ 18 kg/mol), the films were too fragile to float on water and deposit on TEM grids. For that reason, TEM specimens of the 2.7 kg/mol polystyrene were spin-coated directly on silicon-supported Si_3N_4 membranes (window size 1.0 mm, membrane thickness 100 nm, Structure Probe, Inc.). UV−visible absorption spectra were measured on an Agilent Cary 5000 spectrophotometer. Ten transmission electron micrographs were taken (JEOL JEM 2010 TEM, 200 kV) for each sample to provide ample statistics. Because of the thickness of the Si_3N_4 membranes, the TEM images for PS-Au(48):Au(26) had poor contrast, and quantitative analysis was not possible.

Monte Carlo simulations: To model the morphology of the nanocomposites, we adopted a Monte Carlo (MC) model[17,18] which simulates dispersions of polymer-functionalized nanoparticles in an implicit solvent using parameters obtained from classical DFT calculations of the polymer-mediated nanorod−nanorod interactions. Using this implicit solvent approximation, nanoparticles interact via a potential

$$U(h) = \begin{cases} \infty, & h < h_{min} \\ -\varepsilon, & h_{min} \le h \le h_c \\ 0, & h > h_c \end{cases}$$

where h is the distance between the two nanorod surfaces, ε is the nanorod interaction energy, and the cutoff distance in terms of the nanorod radius is $h_c = r_{rod}$. The effect of the polymer brush on the NR spacing is captured by h_{min}, which is taken to be $0.28r_{rod}$. The interaction energies are estimated from DFT calculations by Frischknecht,[10] but for parameters more relevant to the PS-Au(N):PS(P) system ($r_{rod}/R_g \approx 3.0$, $L_{rod}/R_g \approx 22$, and $\sigma \approx 0.5$ chains/nm^2.) For this case where P is not too much larger than N (e.g., $P \approx 2N$), we find $\varepsilon \approx 5k_BT$ (moderate attraction). For larger values of P, ε increases further, and the DFT calculations predict a relatively large attraction between nanorods of $\varepsilon \approx 10k_BT$ for the case of $P \approx 3N$ (i.e., strong attraction). The DFT predicts very weak attractions for $P \lesssim N$, so $\varepsilon = 0$ for this case. The nanorods are constructed from subparticles arranged in a face-centered cubic lattice with a lattice constant of $a = 0.5r_{rod}$ and are randomly dispersed in a thin film with dimensions $256 \times 256 \times 4r_{rod}^3$. Following a short equilibration period, four MC moves are attempted with probabilities of 0.175:0.525:0.15:0.15. These moves correspond to rotation of nanorods, translation of nanorods, rotation of aggregates of nanorods, and translation of aggregates of nanorods, respectively. These moves are accepted according to the Metropolis algorithm at a temperature $T^* = k_BT$. To eliminate statistical deviations, five independent runs with different initial rod positions are executed for each set of parameters. The morphology of the films determined using between 10^6 and 10^7 MC steps were found to be identical. However, this morphology does not represent the final equilibrium morphology, but rather an intermediate, metastable morphology that is representative of experimental conditions. We note that for interaction energies of order $10k_BT$, the final morphology should show macroscopic phase separation of nanorods and polymer; however, because this transition occurs very slowly, MC simulations and experiments fail to reach the final morphology. Finally, our simulations were carried out in a massively parallel fashion using the Compute Unified Device Architecture (CUDA) libraries from NVIDIA on NVIDIA GTS 450 (192 CUDA cores, 1.7 GHz) and NVIDIA GTX 470 (448 CUDA cores, 1.4 GHz) graphics cards. This approach reduced the computation time by approximately two months versus an OpenMP implementation on 4−6 AMD Phenom II cores (2.8 GHz).

Discrete dipole approximation calculations: Discrete dipole approximation (DDA) calculations were performed to determine the extinction efficiencies of dimers and tetramers of Au NRs immersed in a polystyrene matrix as a function of the interparticle separation and wavelength using DDSCAT 7.1 compiled with OpenMP support.[19,20] The extinction efficiency (Q_{ext}) is the sum of the scattering and absorption efficiencies, Q_{sca} and Q_{abs}, respectively. The criterion for accuracy within 5% is that $|m|kd < 0.05$, where m is the complex refractive index, k is the wavenumber, and d is the effective particle size.[3,20] For our calculations, the gold is embedded in a matrix with an average refractive index of 1.55, and the nanorods are represented by approximately 8000 dipoles corresponding to $|m|kd \approx 0.01$. Dielectric data were obtained from Weaver et al.[21] and corrected for surface damping due to collisions of electrons with the surface of the nanorod.[3,22] The extinction efficiencies were determined by taking the average value for light polarized parallel and perpendicular to the length of the nanorods.

dx.doi.org/10.1021/mz200031g | ACS Macro Lett. 2012, 1, 115−121

AUTHOR INFORMATION

Corresponding Author

*E-mail: composto@seas.upenn.edu.

Notes

The authors declare no competing financial interest.

ACKNOWLEDGMENTS

This work was supported by the National Science Foundation with primary support from the Polymer (DMR09-07493), MRSEC (DMR05-20020), and IGERT (DGE-0221664) Programs. Secondary support was provided by NSF/NSEC (DMR08-32802). This work was performed, in part, at the Center for Integrated Nanotechnologies, a U.S. Department of Energy, Office of Basic Energy Sciences user facility. Sandia National Laboratories is a multi-program laboratory managed and operated by Sandia Corporation, a wholly owned subsidiary of Lockheed Martin Corporation, for the U.S. Department of Energy's National Nuclear Security Administration under contract DE-AC04-94AL85000.

REFERENCES

(1) Stockman, M. I. *Phys. Today* **2011**, *64*, 39−44.
(2) Kneipp, K. *Phys. Today* **2007**, *60*, 40−46.
(3) Funston, A. M.; Novo, C.; Davis, T. J.; Mulvaney, P. *Nano Lett.* **2009**, *9*, 165.
(4) Hore, M. J. A.; Composto, R. J. *ACS Nano* **2010**, *4*, 6941−6949.
(5) Liu, Y.; Rafailovich, M. H.; Sokolov, J.; Schwarz, S. A.; Zhong, X.; Eisenberg, A.; Kramer, E. J.; Sauer, B. B.; Satija, S. *Phys. Rev. Lett.* **1994**, *73*, 440.
(6) Bansal, A.; Yang, H.; Li, C.; Benicewicz, R.; Kumar, S.; Schadler, L. *J. Polym. Sci., Part B: Polym. Phys.* **2006**, *44*, 2944.
(7) Shull, K. R. *Faraday Discuss.* **1994**, *98*, 203.
(8) Ferreria, P. G.; Ajdari, A.; Leibler, L. *Macromolecules* **1998**, *31*, 3994.
(9) Matsen, M. W.; Gardiner, J. M. *J. Chem. Phys.* **2001**, *115*, 2794−2804.
(10) Frischknecht, A. L. *J. Chem. Phys.* **2008**, *128*, 224902.
(11) Trombly, D. M.; Ganesan, V. *J. Chem. Phys.* **2010**, *133*, 154904.
(12) Kim, J.; Green, P. F. *Macromolecules* **2010**, *43*, 1524−1529.
(13) Ahmed, W.; Kooij, E. S.; van Silfhout, A.; Poelsema, B. *Nano Lett.* **2009**, *9*, 3786−3794.
(14) Nikoobakht, B.; El-Sayed, M. A. *Chem. Mater.* **2003**, *15*, 1957.
(15) Sau, T. K.; Murphy, C. J. *Langmuir* **2004**, *20*, 6414.
(16) Deshmukh, R. D.; Liu, Y.; Composto, R. J. *Nano Lett.* **2007**, *7*, 3662−3668.
(17) Striolo, A. *Nanotechnology* **2008**, *19*, 445606.
(18) Akcora, P.; et al. *Nat. Mater.* **2009**, *8*, 354.
(19) Flatau, P. J. *J. Opt. Soc. Am. A* **1994**, *11*, 1491.
(20) Draine, B. T.; Flatau, P. J. *User Guide to the Discrete Dipole Approximation Code DDSCAT 7.1* 2010, arXiv.org e-Print archive. http://arXiv.org/abs/1002.1505v1 (accessed Mar 3, 2011).
(21) Weaver, J.; Krafka, C.; Lynch, D.; Koch, E. *Physics Data: Optical Properties of Metals, Part 2: Noble Metals, Aluminium, Scandium, Yttrium, the Lanthanides and the Actinides*; Fach-Informations Zentrum: Karlsruhe, 1981.
(22) Ungureanu, C.; Rayavarapu, R. G.; Manohar, S.; van Leeuwen, T. G. *J. Appl. Phys.* **2009**, *105*, 102032.